INORGANIC CHEMISTRY
FRONTIERS

RESEARCH ARTICLE

View Article Online
View Journal | View Issue

Cite this: *Inorg. Chem. Front.*, 2024, **11**, 8837

Multifunctional separator modified with catalytic multishelled structural CoS_2 enables a stable lithium–sulfur battery†

Ruyi Bi,[a,b] Jilu Zhao,[b,c,d] Mei Yang,[b,c] Jiangyan Wang, *[b,c,d] Ranbo Yu *[a] and Dan Wang *[b,c,d,e]

Lithium–sulfur batteries have been considered as promising next-generation energy storage devices due to their ultrahigh theoretical energy density and natural abundance of sulfur. However, the shuttle effect and sluggish redox kinetics of polysulfides hinder their commercial applications. Herein, by combining smart material design and structure engineering, a CoS_2 hollow multishelled structure (HoMS) has been developed to modify the separator and establish a "vice electrode", which effectively hinders the shuttle effect and catalyzes redox reactions. CoS_2 HoMS can not only obstruct polysulfides through multiple shell barriers but also provide a large available polar surface to effectively capture polysulfides. Additionally, CoS_2 HoMS, with good conductivity, could greatly accelerate the redox conversion of polysulfides and enhance the decomposition of Li_2S. Moreover, CoS_2 HoMS can buffer the large volume change of sulfur during cycling, ensuring good contact and stability of the electrodes. As a result, the lithium–sulfur battery with the CoS_2 HoMS-modified separator exhibited a high discharge capacity of 873.1 mA h g^{-1} at a high rate of 1 C, with only 0.054% capacity decay per cycle during 350 cycles.

Received 14th September 2024,
Accepted 28th October 2024

DOI: 10.1039/d4qi02340d

rsc.li/frontiers-inorganic

The development of advanced energy storage technologies is critical for a sustainable energy future.[1–3] Among existing energy storage systems, lithium–sulfur (Li–S) batteries with their high theoretical energy density (2600 W h kg^{-1}) have been recognized as a promising alternative to traditional Li-ion batteries.[4–7] Meanwhile, the natural abundance, low cost, and nontoxic nature of sulfur make it highly suitable for industrial applications.[8,9] However, the practical application of Li–S batteries suffers from low sulfur utilization and rapid capacity attenuation. These issues mainly originate from the insulation of sulfur and its lithiation products (Li_2S_2/Li_2S), the dissolution and migration of lithium polysulfides (LiPSs) (Li_2S_x, $4 \leq x \leq 8$) (known as the "shuttle effect"), and the large volume variation during the lithiation/delithiation processes.[10,11]

Various strategies, such as sulfur host design,[12–14] new electrolyte additives,[15–17] and separator modification,[18,19] have been developed to improve the conductivity of the integral electrode and inhibit the shuttle effect of LiPSs. All of these approaches have significantly enhanced the electrochemical performance of Li–S batteries. Recently, coating functional materials on a commercial polypropylene (PP) separator as multifunctional interlayers has proven to be a simple and effective approach to suppress the shuttle effect and improve the redox kinetics of sulfur species.[20,21] Carbonaceous materials with their high conductivity and large surface area have attracted much attention for efficiently reutilizing polysulfides dissolved in electrolytes, such as meso-/microporous carbon,[22] carbon nanotube,[23] graphene/graphene oxide,[24] and graphdiyne.[25] However, the performance improvement is limited due to the weak affinity between nonpolar carbon materials and polar LiPSs. Many researchers have focused on strengthening the chemical barriers by heteroatom doping carbonaceous materials[26–29] or utilizing some polar inorganics.[30–32] The limited adsorption of the heteroatom and poor conductivity of these inorganics lead to limited improved electrochemistry performance. Generally, the accumulation of LiPS intermediates in the electrolyte cause the polysulfide shuttling effect. The sluggish conversion kinetics between the soluble LiPSs and insoluble final products will aggravate this phenomenon.[33] An electrocatalyst that can accelerate the reaction between soluble LiPS intermediates and insoluble Li_2S_2/

[a]*School of Metallurgical and Ecological Engineering, University of Science and Technology Beijing, Beijing 100083, China. E-mail: ranboyu@ustb.edu.cn*
[b]*State Key Laboratory of Biochemical Engineering, Institute of Process Engineering, Chinese Academy of Sciences, Beijing 100190, China. E-mail: jywang@ipe.ac.cn, danwang@ipe.ac.cn*
[c]*Key Laboratory of Biopharmaceutical Preparation and Delivery, Chinese Academy of Sciences, Beijing 100190, China*
[d]*School of Chemical Engineering, University of Chinese Academy of Sciences, Beijing 100049, China*
[e]*College of Chemistry and Environmental Engineering, Shenzhen University. E-mail: danwang@szu.edu.cn*
† Electronic supplementary information (ESI) available. See DOI: https://doi.org/10.1039/d4qi02340d

Li_2S seems to prevent the shuttling of LiPSs. Hence, the important role of electrocatalysts in Li–S batteries has drawn much research attention.[34–36] Among these reported catalyst, such as metal or conductive compounds, the half-metallic CoS_2 with high electrical conductivity (6.7×10^3 S cm^{-1} at 300 K) and high electrocatalytic activity can enhance the redox kinetics of LiPSs, thus attenuating the shuttle effect and improving the electrochemical properties.[37–40]

Interface engineering is also important for catalytic materials to provide much more catalytically active sites that promote the redox kinetics of the polysulfide.[19,41] Among many structures, hollow multishelled structures (HoMS) have shown tremendous promise as electrode materials for lithium ion batteries due to their outstanding advantages, such as the shortened charge transport path and buffer volume change.[42–47] The Wang group first reported the synthesis of HoMS of metal ferrite in 2009.[48] They synthesized TiO_{2-x} HoMS[49] and NiO HoMS,[50] which were applied as sulfur hosts and showed stable cycling performances.

Herein, by combining the wisdom of material design and structure engineering, we developed CoS_2 HoMSs to modify the separator of the Li–S battery. Benefiting from the compositional advantages of CoS_2 and structural advantages of HoMS, the key challenges of the Li–S battery could be efficiently addressed. As shown in Scheme 1, CoS_2 HoMS can not only obstruct LiPSs as a kind of multistep physical barrier, but the larger available polar surface area of the hollow structures also enables better trapping of LiPSs. With its appreciable conductivity, the half-metallic CoS_2 can accelerate the polysulfide redox conversion and Li_2S decomposition to enhance the reutilization of the sulfur species. Moreover, the hollow interior can act as a buffer space to accommodate the large sulfur volume expansion, thus stabilizing the electrode and further improving the cycling stability.

CoS_2 HoMS is synthesized *via* a facile thermal treatment method from the sulfuration of Co_3O_4 HoMS (Fig. S1–S3†). The morphology of CoS_2 HoMS still retains the same dimensions after treatment (Fig. 1a–c). The scanning electron microscopy (SEM) image (Fig. 1d) shows that 3S-CoS_2 HoMS has a rather uniform size distribution. The inserted image of the broken sphere proves the hollow interior of CoS_2 HoMS. The lattice distance of 0.27 nm measured from the HRTEM image (Fig. 1e and f) was consistent with the (200) facet, and demonstrated the highly crystalline nature of the as-prepared CoS_2 HoMS. As further proved by XRD (Fig. 1g), all reflection peaks display a typical pyrite-type structure (JCPDS card no. 65-3322, space group: $Pa\bar{3}$ (205), α = 5.538 Å), with no additional peaks detected. X-ray photoelectron spectroscopy (XPS) was employed to characterize the composition and chemical states of the as-synthesized CoS_2 HoMS. The XPS survey spectra in Fig. S4† proved the existence of S, C, O, and Co. The high-resolution spectra of Co 2p are shown in Fig. 1h, and were fitted with two spin–orbit doublets (Co 2p1/2 and Co 2p3/2) and two shake-up satellites. The peaks at 778.32 and 793.43 eV are assigned to the trivalent state of Co. The peaks at 780.52 and 796.74 eV are assigned to the divalent state, and the oxidized species in the CoS_2 samples originate from the partial surface oxidization.[39,51] Further analysis of the high-resolution S 2p spectra is shown in Fig. 1i. In the S 2p spectra, two peaks at 162.29 and 163.50 eV coincide with the binding energies of the Co–S bond. Meanwhile, the high intensity peaks at 168.01 and 169.21 eV are attributed to the existence of the S–O group. The S_2^{2-} peaks at 162.70 and 164.81 eV indicate the presence of unsaturated sulfur atoms on the surface.[52]

CoS_2 HoMS with carbon nanotubes (CNT) in a mass proportion of 6 : 1 was coated on a single side of a commercial PP separator through vacuum filtration. The approximate loading of the total material is 0.33 mg cm^{-2}. Fig. 2a shows the sche-

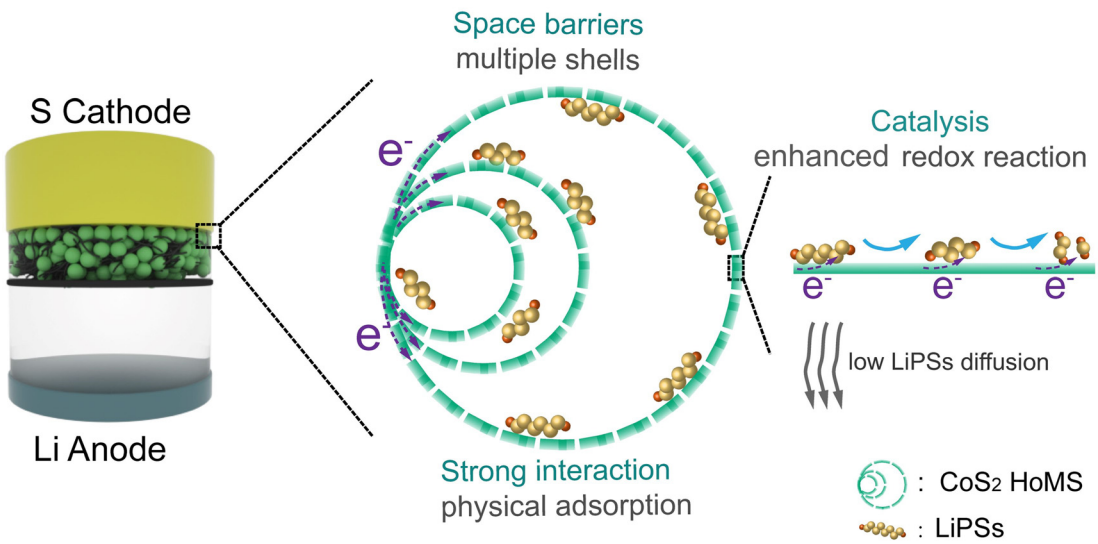

Scheme 1 Scheme showing the CoS_2 HoMS-modified separator for inhibiting the shuttle effect of LiPSs and enhancing the redox conversion of the S cathode.

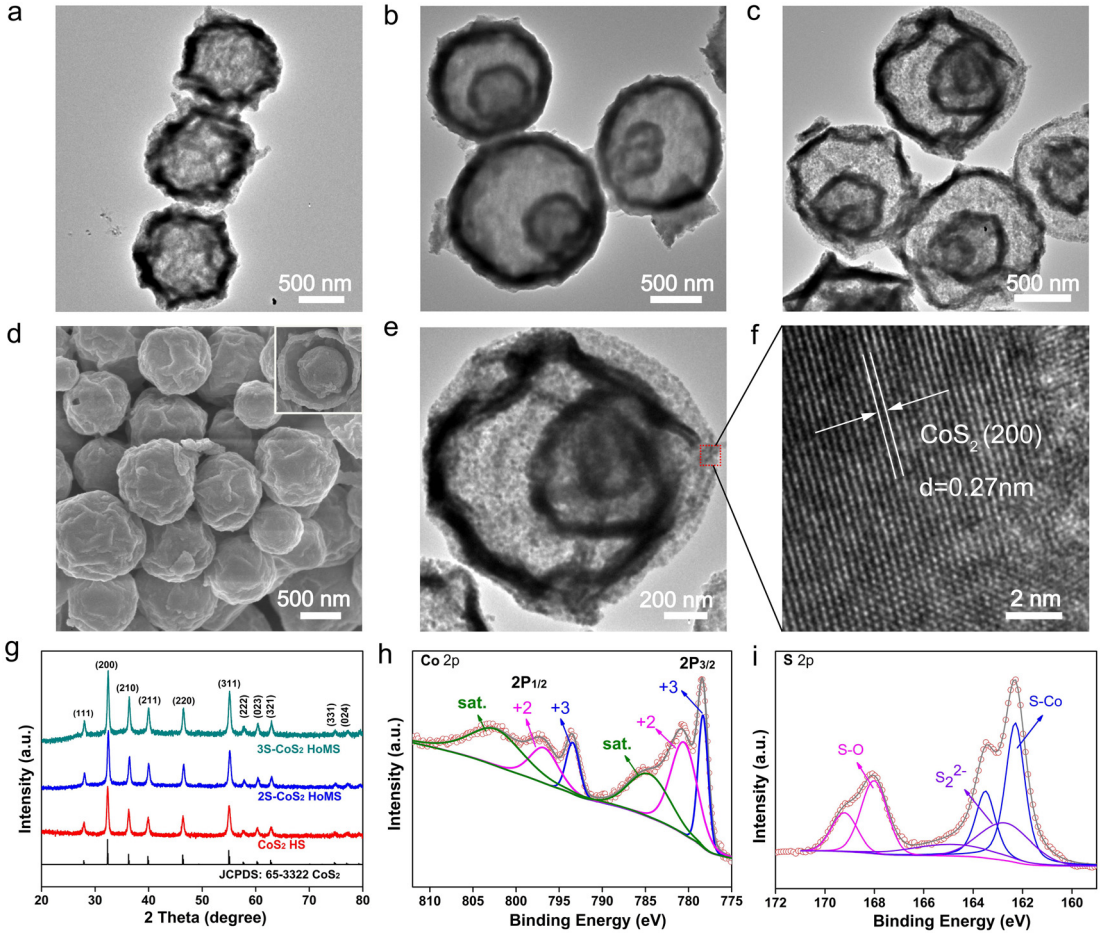

Fig. 1 The composition and structural characterization of CoS_2 HoMS. TEM images of the (a) single (1S-), (b) double (2S-), and (c) triple (3S-) shelled CoS_2 HoMS. (d) SEM image of 3S-CoS_2 HoMS with an inset image of a broken sphere showing the multishelled structure. (e) TEM and (f) HRTEM images of an individual 3S-CoS_2 HoMS. (g) XRD patterns of the as-prepared samples. (h and i) XPS spectra of the Co 2p peaks (h) and S 2p peaks (i).

matic diagram of the CoS_2 HoMS-coated separator (CoS_2 HoMS@PP). The vacuum filtration deposition process (Fig. 2b) results in excellent adhesion of CoS_2 HoMS to the commercial separator, and shows the characteristic diffraction peaks of CoS_2 by XRD characterization (Fig. S5†). The structure of the integrated electrode was further examined by SEM and EDX mapping. The top-view SEM image clearly shows that CoS_2 HoMS and CNT are connected (Fig. 2c and Fig. S6†). A cross-section SEM image revealed the layer structure of the densely compact CoS_2 HoMS film with a thickness of ~6.1 μm (Fig. 2d), and the EDX elemental mapping revealed the distribution of Co, S, and C in the integrated electrode. The intrinsic hydrophilicity of the CoS_2 HoMS coatings greatly improved the wettability of the separators. We also prepared CoS_2 NP as a comparative study (CoS_2 NP@PP, Fig. S7 and S8†). As shown in Fig. 2e–g, it can be clearly observed that the contact angle of the PP separator almost remains unchanged after 10 seconds. Meanwhile, the CoS_2 NP-coated separator disappears after 1 second, while the contact angle of the CoS_2 HoMS-coated separator disappeared within 0.5 seconds. The improved wetting may be ascribed to the capillary effect of CoS_2 HoMS. The improved surface wettability is expected to benefit the separator/electrode interfacial compatibility and increase the electrolyte retention in the separator, which facilitates Li-ion diffusion through the separator and improves the electrochemical performance of the Li–S batteries, especially at high rates.[53–55]

A symmetric battery with identical working and counter electrodes in 0.5 M Li_2S_6 electrolyte was assembled to demonstrate the electrocatalysis activity of different materials (Fig. S9†). As a CNT that is used in S cathodes and interlayer may influence the electrochemistry process, we intentionally included the CV and EIS data of the CNT for a clear comparison of the catalytic activity. As shown in Fig. 3a, the battery without Li_2S_6 shows near-zero capacitive current density without any obvious redox peaks. After adding Li_2S_6, the battery exhibits four pronounced reduction/oxidation peaks. Those peaks can be assigned to the diverse electrochemical reactions of LiPSs on the electrodes.[56] The CV of the CNT electrode also shows four reduction/oxidation peaks, but the current densities of these peaks are significantly lower. Furthermore, the voltage hysteresis between the cathodic and

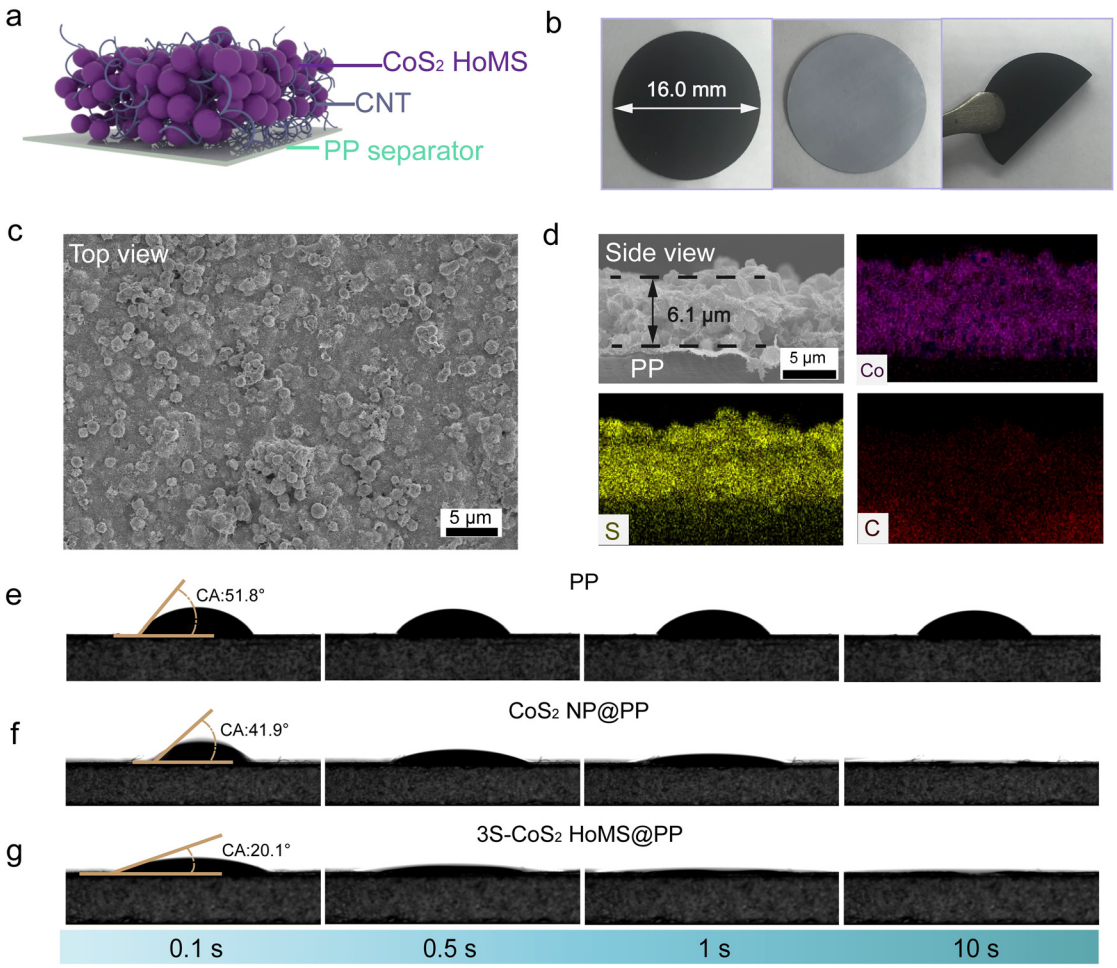

Fig. 2 The morphology and wettability characterization of different separators. (a) Schematic diagram of the CoS_2 HoMS-coated separator. (b) Optical photographs, (c) top-view, and (d) cross-section SEM images of the 3S-CoS_2 HoMS-coated separator. (e–g) Comparison of the contact angles of PP (e), CoS_2 NP (f) and 3S-CoS_2 HoMS (g) coated separator at different contact times.

anodic peaks is much higher than that for the 3S-CoS_2 HoMS electrode. It is also found that the 3S-CoS_2 HoMS electrode has a smaller charge transfer resistance from the EIS test (Fig. 3b and Table S1†). This result clearly indicates that the 3S-CoS_2 HoMS can effectively facilitate charge transfer and enhance the kinetics of LiPSs. Simultaneously, the diffusion coefficients of Li ions with the PP separator and 3S-CoS_2 HoMS-coated separator were characterized by CV with different sweep rates (Fig. 3c–e). The lithium ion diffusion coefficients were calculated according to the Randles–Sevick equation.[57,58] It can be clearly seen that the diffusion coefficients of the 3S-CoS_2 HoMS-coated separator are higher than that of the PP separator in each redox peak (Fig. 3f and Table S2†). Consequently, the lithium ion transfer that occurred after modifying the separator was accelerated rather than hindered. This can be attributed to the micro/mesopores and multi-shell structure of 3S-CoS_2 HoMS, which enhances the electrolyte wettability and shortens the lithium ion transfer path.

The effect of CoS_2 HoMS on the precipitation of Li_2S was also studied. Cells were assembled using a 3S-CoS_2 HoMS-loaded carbon fiber cloth (CFC) or bare CFC as the cathode and lithium metal as the anode. Cells were discharged to 2.06 V at a current density of 0.112 mA, and then the potential was held at 2.05 V until the current dropped below 0.01 mA. As shown in Fig. S10,† the deposition capacity of Li_2S on the surface of the 3S-CoS_2 HoMS-loaded CFC is much larger than that on bare CFC, confirming that 3S-CoS_2 HoMS can enhance the conversion of polysulfides to Li_2S and the nucleation and growth of Li_2S. The reasons may be ascribed to 3S-CoS_2 HoMS accelerating the redox reactions of polysulfides, and also enhancing the deposition of Li_2S.

The electrochemical performance of the Li–S battery using the PP separator, CoS_2 NP, and CoS_2 HoMS-coated separator is shown in Fig. 4. In the initial cathodic scan of the cyclic voltammetry (CV) curves with the PP separator (Fig. 4a), the CV curves show two distinct cathodic peaks located at around 2.30 V and 2.01 V, corresponding to the reduction of S_8 to lithium polysulfide (Li_2S_x, x = 4–8), and the subsequent reduction to insoluble Li_2S_2/Li_2S, respectively. In the subsequent anodic scan, the oxidation peaks at approximately 2.34 V and 2.43 V

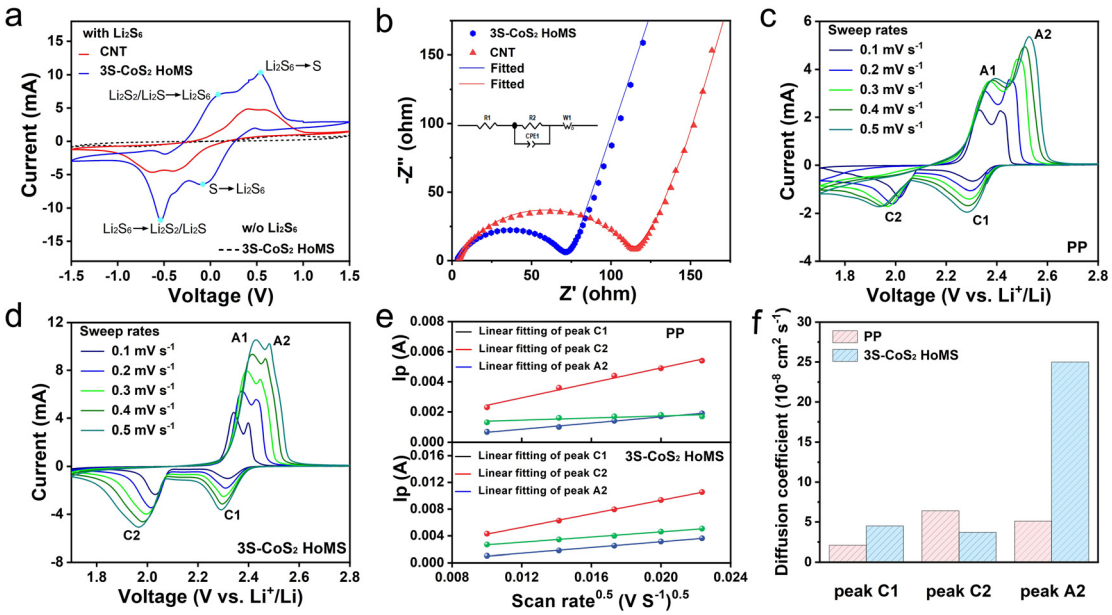

Fig. 3 Comparison of the kinetic behaviors of batteries using different separators. (a) CV curves at a scan rate of 5 mV s^{-1} and (b) EIS spectra of the Li_2S_6 symmetric battery, employing CNT and 3S-CoS_2 HoMS as the identical electrodes. (c–e) CV curves of the Li–S cells with the PP separator (c) and 3S-CoS_2 HoMS-coated separator (d) at different scan rates from 0.1 to 0.5 mV s^{-1}, and (e) corresponding linear fits of the peak currents. (f) Comparison of lithium ion diffusion coefficients for the Li–S batteries.

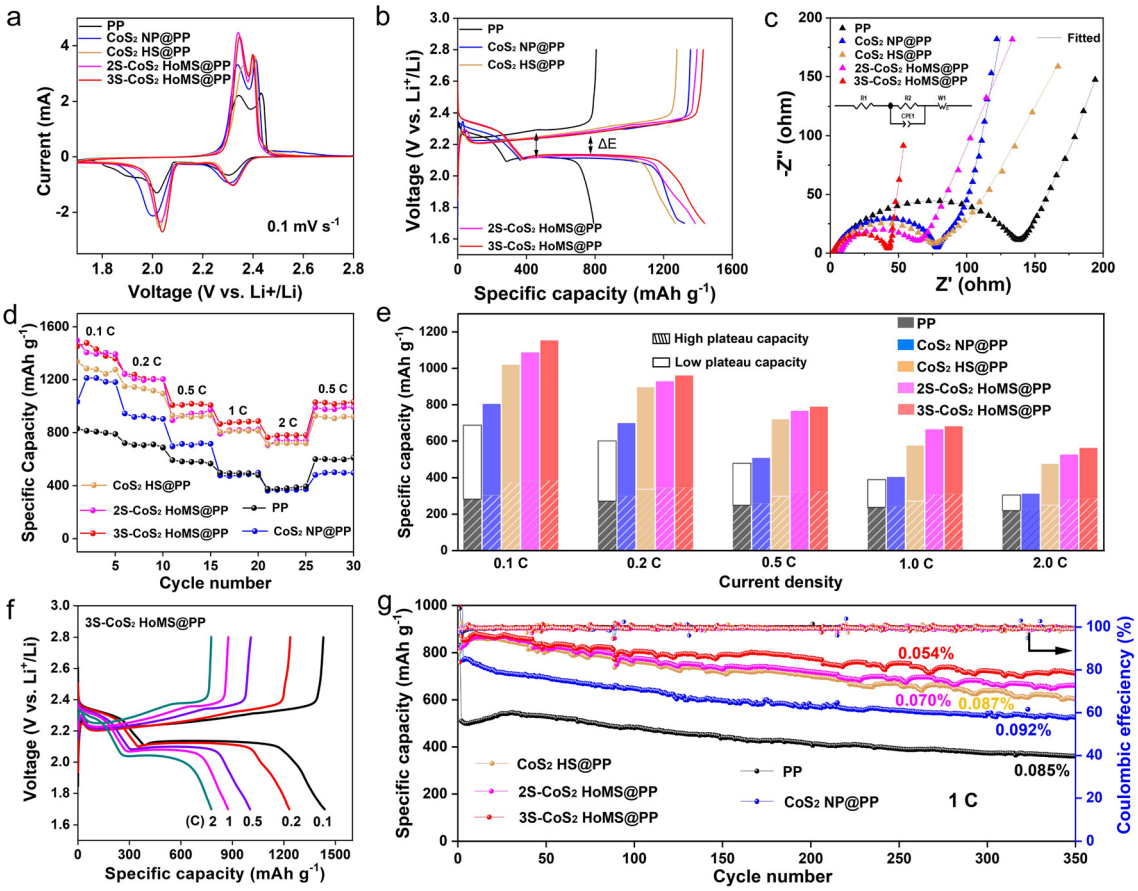

Fig. 4 Electrochemical performance of cathodes with different separators. (a) CV curves at the scan rate of 0.1 mV s^{-1}. (b) The first-cycle galvanostatic charge–discharge profiles at 0.1 C. (c) EIS spectra. (d) The rate capability of the Li–S batteries. (e) High and low plateau capacities at different current densities. (f) Galvanostatic charge–discharge profiles of the 3S-CoS_2 HoMS-coated separator at various current densities. (g) Long cycle performance at a current density of 1 C with the capacity decay rate labeled.

are ascribed to the delithiation of Li_2S_2/Li_2S and Li_2S_x (x = 4–8), respectively, to form the final elemental sulfur.[33] All samples show similar CV profiles. However, the batteries with CoS_2-modified separators with different morphologies show a narrower potential separation between the anodic and cathodic peaks and higher peak current density, implying that the CoS_2 interlayer can efficiently reduce the resistance and promoted redox kinetics of the sulfur electrode.[35] Fig. 4b shows the charge/discharge profiles of different electrodes, which are consistent with the results of the CV test showing two distinct plateaus of the sulfur electrode. The batteries with CoS_2-modified separators with different morphologies had a voltage hysteresis (ΔE) that was lower than that of the commercial PP separator. Moreover, 3S-CoS_2 HoMS shows the minimum ΔE corresponding to the CV results, indicating highly efficient redox reactions, thus increasing the utilization of sulfur materials.[59–62] Furthermore, electrochemical impedance spectra (EIS) measurements reveal that the batteries with the CoS_2-modified separator show a smaller charge transfer resistance in the high-frequency region than the commercial PP separator, and the impedance decreases with increasing shell number (Fig. 4c and Table S3†). This result coincides with the previous article mentioning the large electrolyte/electrode contact area.[63,64]

To further investigate the electrochemical performance of the electrode at different current densities, the rate performance of the battery with different separators was tested at a series of rates from 0.1 C to 2 C (Fig. 4d). Compared to the low specific capacities of the battery with the PP separator and CoS_2 NP-coated separator at different current densities, the battery with the 3S-CoS_2 HoMS-coated separator delivered much higher specific capacities of 1438, 1198, 1014, 877, and 776 mA h g^{-1} at 0.1, 0.2, 0.5, 1, and 2 C, respectively. When the current rate was changed back to 0.5 C again, the discharge capacity of the 3S-CoS_2 HoMS-coated separator increases to 1112 mA h g^{-1}, thus demonstrating excellent rate performance and capacity retention, especially at high current density. Moreover, when calculating the capacity contribution between the high and low plateau capacities at different current densities, it is worth noting that the 3S-CoS_2 HoMS-coated separa-

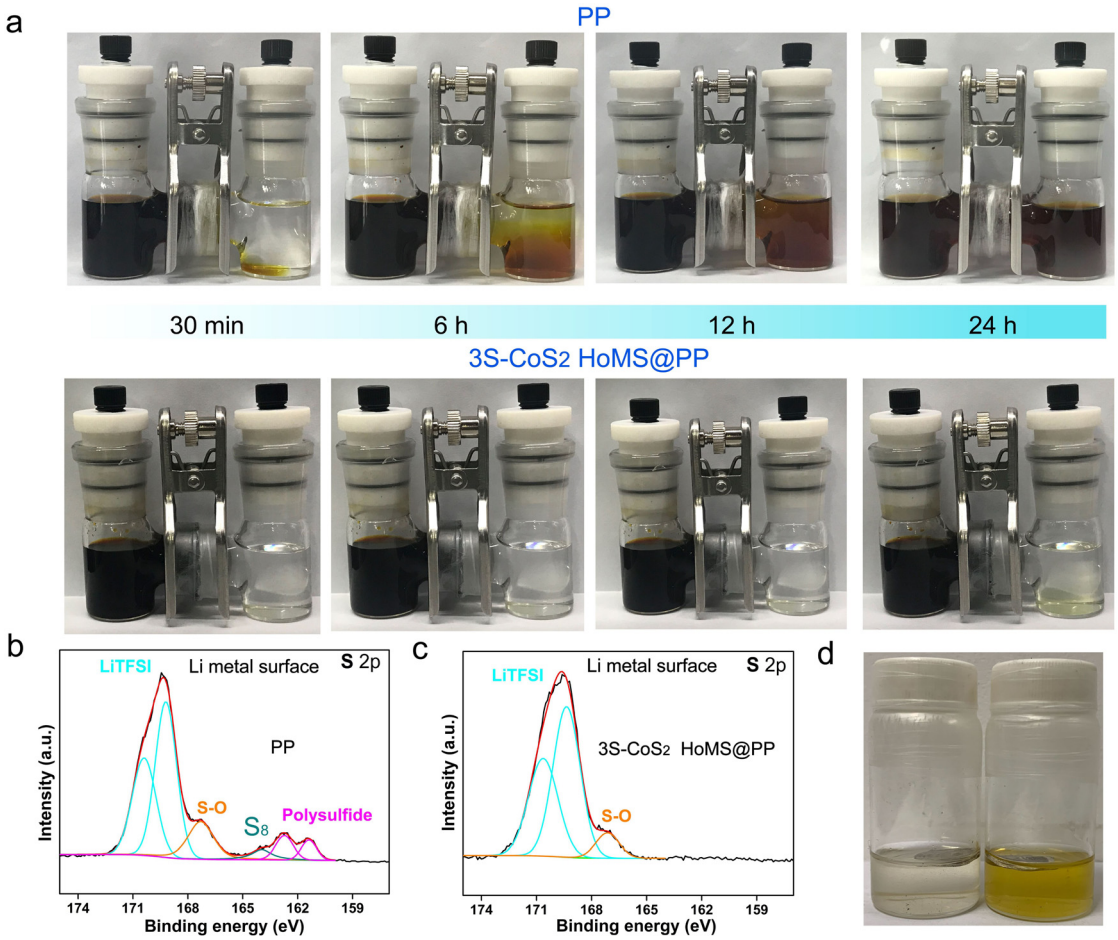

Fig. 5 Comparison of the inhibition of the shuttle effect using different separators. (a) Optical photographs of the LiPS permeation test in the H-type glass vessel for the PP separator (top) and 3S-CoS_2 HoMS-coated separator (down) at different times. (b and c) XPS spectra of the Li metal with the PP separator and 3S-CoS_2 HoMS-coated separator after 100 cycles at 1 C. (d) Photographs of the cycled Li metal foil (at the state of charge) with the PP separator (left) and 3S-CoS_2 HoMS-modified separator (right) in the electrolyte.

tor has a larger capacity contribution from the high and low plateau ranges, especially at high current densities when compared with other samples (Fig. 4e). In addition, it is clearly observed that the two discharge/charge plateaus are well-retained even at a high rate of 2 C (Fig. 4f), which is different from the commercial PP separator electrode wherein the plateaus disappear at high current density (Fig. S11†). This result indicates that the 3S-CoS_2 HoMS-coated separator electrode possesses excellent reaction kinetics.[35]

To exclude the capacity contribution from CoS_2 HoMS, we directly assembled a battery that uses 2S-CoS_2 HoMS as the electrode material. The results show that the capacity is almost negligible in the potential range (Fig. S12†). The cycle performance of different separators was tested at 1.0 C between 1.5 and 2.8 V for 350 cycles, as shown in Fig. 4g. Among all the electrodes with different separators, the battery with the 3S-CoS_2 HoMS-coated separator exhibits the best performance, achieving the highest initial discharge capacity of 873.1 mA h g^{-1}, which maintained 707.3 mA h g^{-1} after 350 cycles (corresponding to a capacity decay of 0.054% per cycle). The first discharge capacities of the 2S-CoS_2 HoMS, CoS_2 HS, and CoS_2 NP-coated separator electrodes are 866.5, 861.6, and 775 mA h g^{-1}, respectively. Furthermore, the discharge capacities after 350 cycles are 655.6, 597.9, and 525 mA h g^{-1}, respectively (the corresponding capacity decays per cycle are 0.070%, 0.087% and 0.092%, respectively). The battery with the PP separator delivers a minimum initial discharge capacity of 510.1 mA h g^{-1}, and falls to 359.0 mA h g^{-1} after 350 cycles (corresponding to a capacity decay of 0.085% per cycle). This is mainly because the multilayer surface of CoS_2 HoMS can provide adsorption sites for LiPSs, and the multiple domain spatial confinement of HoMS further improves the redox reaction kinetics of LiPSs, so as to reduce the residence time of LiPSs in the electrolyte (Fig. S13†).

To prove the merit of the 3S-CoS_2 HoMS interlayer in prohibiting the polysulfide diffusion, the polysulfide permeability test was conducted by an H-type visualized glass vessel (Fig. 5a). 0.1 M Li_2S_6 in dioxolane (DOL)/dimethoxyethane (DME) solvent and pure DOL/DME solvent was separated by PP separator (top), and 3S-CoS_2 HoMS-coated PP separator (bottom), respectively. The right of the glass vessel with the PP separator displays an obvious dark yellow color after 6 h. In contrast, there is little color change based on the 3S-CoS_2 HoMS-coated PP separator after 24 h. These results reveal that the shuttling phenomenon of LiPSs was suppressed by the 3S-CoS_2 HoMS interlayer. From the XPS of the Li metal after 100 cycles at 1 C presented in Fig. 5b and c, the S–S and Li–S bonding species appeared on the Li metal with PP as the separator, indicating the existence of LiPSs.[18] However, the content of these species with the 3S-CoS_2 HoMS-coated separator is very low, suggesting that the shuttle phenomenon is blocked by the interlayer. This inhibited shuttle effect can also be confirmed by comparing the Li metal color (Fig. 5d and Fig. S14†). The solution in the right glass vessel corresponding to the one with the 3S-CoS_2 HoMS-coated PP separator is much cleaner than that in the left one with the bare PP separator.

Conclusion

In summary, CoS_2 HoMSs have been developed to modify the separator and form a multifunctional interlayer for high performance Li–S batteries. The multiple shells of CoS_2 HoMS can serve as multiple physical barriers to suppress the polysulfide shuttle and the inner cavity can accommodate LiPSs. Furthermore, the polar properties and good conductivity of the CoS_2 materials can effectively trap LiPSs and enhance the redox reactions. As a result, the battery with 3S-CoS_2 HoMS-modified separator exhibited good cyclic performance with a high discharge capacity of 873.1 mA h g^{-1} at a current density of 1 C. Furthermore, it delivered only 0.054% of capacity decay per cycle during 350 cycles, which is superior to the one with the unmodified separator or with the CoS_2 NP-modified separator. This work will inspire novel insight into the design of a multifunctional structure to address the bottleneck of high-energy-density energy storage systems.

Author contributions

D.W. conceived the idea and supervised the research. R.Y. and J.W. supervised the research. R.B. and J. Z. performed the experiments and basic characterizations. D.W., R.Y., J.W., R.B., J. Z. and M.Y. analyzed and discussed the experimental data. J. W. drafted the manuscript. D.W. and R.Y. revised and improved the manuscript. All authors read and approved the final manuscript.

Data availability

The authors confirm that the data supporting the findings of this study are available within the article [and its ESI†]. More detailed data are available on request from the corresponding author, upon reasonable request.

Conflicts of interest

There are no conflicts to declare.

Acknowledgements

This work was supported by the Natural Science Foundation of China (Grant No.: 51932001, 52301296, 52261160573 and 21971245), the National Key R&D Program (Grant No.: 2018YFA0703504, 2022YFA1504101, 2022YFA1204500 and 2022YFA1204502), the Zhongke-Yuneng Joint R&D Center Program (No.: ZKYN2022008), and the Institute of Process Engineering (IPE) Project for Frontier Basic Research (Grant No. QYJC-2022-008).

References

1 F. Pei, L. Lin, A. Fu, S. Mo, D. Ou, X. Fang and N. Zheng, A Two-Dimensional Porous Carbon-Modified Separator for High-Energy-Density Li-S Batteries, *Joule*, 2018, **2**, 323–336.
2 Y. Gao, Q. Guo, Q. Zhang, Y. Cui and Z. Zheng, Fibrous Materials for Flexible Li–S Battery, *Adv. Energy Mater.*, 2021, **11**, 2170058.
3 X. Fan, B. Liu, J. Liu, J. Ding, X. Han, Y. Deng, X. Lv, Y. Xie, B. Chen, W. Hu and C. Zhong, Battery Technologies for Grid-Level Large-Scale Electrical Energy Storage, *Trans. Tianjin Univ.*, 2020, **26**, 92–103.
4 L. Zhou, Z. Zhuang, H. Zhao, M. Lin, D. Zhaoand and L. Mai, Intricate Hollow Structures: Controlled Synthesis and Applications in Energy Storage and Conversion, *Adv. Mater.*, 2017, **29**, 1602914.
5 Y. X. Yin, S. Xin, Y. G. Guo and L. J. Wan, Lithium–Sulfur Batteries: Electrochemistry, Materials, and Prospects, *Angew. Chem., Int. Ed.*, 2013, **52**, 13186.
6 L. Du, H. Wang, M. Yang, L. Liu and Z. Niu, Free-Standing Nanostructured Architecture as a Promising Platform for High-Performance Lithium–Sulfur Batteries, *Small Struct.*, 2020, **1**, 2000047.
7 R. Lu, M. Cheng, L. Mao, M. Zhang, H. Yuan, K. Amin, C. Yang, Y. Cheng, Y. Meng and Z. Wei, Nitrogen-doped nanoarray-modified 3D hierarchical graphene as a cofunction host for high-performance flexible Li-S battery, *EcoMat*, 2020, **2**, e12010.
8 X. Ji, K. T. Lee and L. F. Nazar, A highly ordered nanostructured carbon–sulphur cathode for lithium–sulphur batteries, *Nat. Mater.*, 2009, **8**, 500–506.
9 P. G. Bruce, S. A. Freunberger, L. J. Hardwick and J. M. Tarascon, Li–O_2 and Li–S batteries with high energy storage, *Nat. Mater.*, 2011, **11**, 19–29.
10 S. Zhou, J. Shi, S. Liu, G. Li, F. Pei, Y. Chen, J. Deng, Q. Zheng, J. Li, C. Zhao, I. Hwang, C. J. Sun, Y. Liu, Y. Deng, L. Huang, Y. Qiao, G. L. Xu, J. F. Chen, K. Amine, S. G. Sun and H. G. Liao, Visualizing interfacial collective reaction behaviour of Li–S batteries, *Nature*, 2023, **621**, 75–81.
11 H. Li, R. Meng, C. Ye, A. Tadich, W. Hua, Q. Gu, B. Johannessen, X. Chen, K. Davey and S. Z. Qiao, Developing high-power Li||S batteries via transition metal/carbon nanocomposite electrocatalyst engineering, *Nat. Nanotechnol.*, 2024, **19**, 792–799.
12 G. He, S. Evers, X. Liang, M. Cuisinier, A. Garsuch and L. F. Nazar, Tailoring Porosity in Carbon Nanospheres for Lithium–Sulfur Battery Cathodes, *ACS Nano*, 2013, **7**, 10920–10930.
13 Z. W. Seh, W. Li, J. J. Cha, G. Zheng, Y. Yang, M. T. McDowell, P. C. Hsu and Y. Cui, Sulphur–TiO_2 yolk–shell nanoarchitecture with internal void space for long-cycle lithium–sulphur batteries, *Nat. Commun.*, 2013, **4**, 1331.
14 M. Wang, Y. Han, H. Peng, Z. Jin, H. Guan, S. Ma, X. Li, Y. Ren, L. Xie, X. Zheng, J. Zhang and Y. Dong, Boosting the electrocatalytic activity of 2D ultrathin BiOX/rGO (X = F, Cl, Br, and I) nanosheets as sulfur hosts: insight into the electronegativity effect of halogenated elements on the electrochemical performances of lithium–sulfur batteries, *Inorg. Chem. Front.*, 2024, **11**, 4277–4287.
15 S. Chen, F. Dai, M. L. Gordin, Z. Yu, Y. Gao, J. Song and D. Wang, Functional Organosulfide Electrolyte Promotes an Alternate Reaction Pathway to Achieve High Performance in Lithium-Sulfur Batteries, *Angew. Chem., Int. Ed.*, 2016, **55**, 4231.
16 S. Chen, D. Wang, Y. Zhao and D. Wang, Superior Performance of a Lithium–Sulfur Battery Enabled by a Dimethyl Trisulfide Containing Electrolyte, *Small Methods*, 2018, **2**, 1800038.
17 J. Y. Wei, X. Q. Zhang, L. P. Hou, P. Shi, B. Q. Li, Y. Xiao, C. Yan, H. Yuan and J. Q. Huang, Organosulfur-Containing Solid Electrolyte Interphase on the Lithium Anode in Lithium-Sulfur Batteries, *Adv. Mater.*, 2020, **32**, e2003012.
18 L. Fan, M. Li, X. Li, W. Xiao, Z. Chen and J. Lu, Interlayer Material Selection for Lithium-Sulfur Batteries, *Joule*, 2019, **3**, 361–386.
19 H. Yuan, H. J. Peng, B. Q. Li, J. Xie, L. Kong, M. Zhao, X. Chen, J. Q. Huang and Q. Zhang, Conductive and Catalytic Triple-Phase Interfaces Enabling Uniform Nucleation in High-Rate Lithium–Sulfur Batteries, *Adv. Energy Mater.*, 2019, **9**, 1802768.
20 X. Wang, P. Lin, C. Wu, Y. Zhu, C. Wang, D. Guo, X. A. Chen and S. Wang, Superior-performance lithium–sulfur batteries: a face-centered-cubic-structure high-entropy alloy improves the bidirectional catalytic conversion of polysulfides/sulfides, *Inorg. Chem. Front.*, 2024, **11**, 6425–6437.
21 P. Li, H. Lv, Z. Li, X. Meng, Z. Lin, R. Wang and X. Li, The Electrostatic Attraction and Catalytic Effect Enabled by Ionic–Covalent Organic Nanosheets on MXene for Separator Modification of Lithium–Sulfur Batteries, *Adv. Mater.*, 2021, **33**, e2007803.
22 A. Fu, C. Wang, F. Pei, J. Cui, X. Fang and N. Zheng, Recent Advances in Hollow Porous Carbon Materials for Lithium-Sulfur Batteries, *Small*, 2019, **15**, e1804786.
23 Y. Pang, J. Wei, Y. Wang and Y. Xia, Synergetic Protective Effect of the Ultralight MWCNTs/NCQDs Modified Separator for Highly Stable Lithium–Sulfur Batteries, *Adv. Energy Mater.*, 2018, **8**, 1702288.
24 G. Zhou, L. Li, D. W. Wang, X. Y. Shan, S. Pei, F. Li and H. M. Cheng, A Flexible Sulfur-Graphene-Polypropylene Separator Integrated Electrode for Advanced Li–S Batteries, *Adv. Mater.*, 2015, **27**, 641.
25 Y. Wang, J. He, Z. Zhang, Z. Liu, C. Huang and Y. Jin, Graphdiyne-Modified Polyimide Separator: A Polysulfide-Immobilizing Net Hinders the Shuttling of Polysulfides in Lithium-Sulfur Battery, *ACS Appl. Mater. Interfaces*, 2019, **11**, 35738–35745.
26 G. Zhou, E. Paek, G. S. Hwang and A. Manthiram, Long-life Li/polysulphide batteries with high sulphur loading enabled by lightweight three-dimensional nitrogen/

sulphur-codoped graphene sponge, *Nat. Commun.*, 2015, **6**, 7760.

27 Q. Li, Y. Song, R. Xu, L. Zhang, J. Gao, Z. Xia, Z. Tian, N. Wei, M. H. Rummeli, X. Zou, J. Sun and Z. Liu, Biotemplating Growth of Nepenthes-like N-Doped Graphene as a Bifunctional Polysulfide Scavenger for Li-S Batteries, *ACS Nano*, 2018, **12**, 10240–10250.

28 L. Zhang, D. Liu, Z. Muhammad, F. Wan, W. Xie, Y. Wang, L. Song, Z. Niu and J. Chen, Single Nickel Atoms on Nitrogen-Doped Graphene Enabling Enhanced Kinetics of Lithium–Sulfur Batteries, *Adv. Mater.*, 2019, **31**, 1903955.

29 S. Kong, D. Cai, G. Li, X. Xu, S. Zhou, X. Ding, Y. Zhang, S. Yang, X. Zhou and H. Nie, Hydrogen-substituted graphdiyne/graphene as an sp/sp^2 hybridized carbon interlayer for lithium–sulfur batteries, *Nanoscale*, 2021, **13**, 3817–3826.

30 Z. Xiao, Z. Yang, L. Wang, H. Nie, M. Zhong, Q. Lai, X. Xu, L. Zhang and S. Huang, Lithium-Sulfur Batteries: A Lightweight TiO2/Graphene Interlayer, Applied as a Highly Effective Polysulfide Absorbent for Fast, Long-Life Lithium–Sulfur Batteries, *Adv. Mater.*, 2015, **27**, 2891.

31 Y. Dong, S. Zheng, J. Qin, X. Zhao, H. Shi, X. Wang, J. Chen and Z. S. Wu, All-MXene-Based Integrated Electrode Constructed by Ti_3C_2 Nanoribbon Framework Host and Nanosheet Interlayer for High-Energy-Density Li–S Batteries, *ACS Nano*, 2018, **12**, 2381–2388.

32 K. Chen, G. Zhang, L. Xiao, P. Li, W. Li, Q. Xu and J. Xu, Polyaniline Encapsulated Amorphous V_2O_5 Nanowire-Modified Multi-Functional Separators for Lithium–Sulfur Batteries, *Small Methods*, 2021, **5**, 2001056.

33 L. Peng, Z. Wei, C. Wan, J. Li, Z. Chen, D. Zhu, D. Baumann, H. Liu, C. S. Allen, X. Xu, A. I. Kirkland, I. Shakir, Z. Almutairi, S. Tolbert, B. Dunn, Y. Huang, P. Sautet and X. Duan, A fundamental look at electrocatalytic sulfur reduction reaction, *Nat. Catal.*, 2020, **3**, 762–770.

34 Y. Song, W. Cai, L. Kong, J. Cai, Q. Zhang and J. Sun, Rationalizing Electrocatalysis of Li–S Chemistry by Mediator Design: Progress and Prospects, *Adv. Energy Mater.*, 2019, **10**, 1901075.

35 Z. Shi, Z. Sun, J. Cai, Z. Fan, J. Jin, M. Wang and J. Sun, Boosting Dual-Directional Polysulfide Electrocatalysis via Bimetallic Alloying for Printable Li–S Batteries, *Adv. Funct. Mater.*, 2020, **31**, 2006798.

36 B. Q. Li, H. J. Peng, X. Chen, S. Y. Zhang, J. Xie, C. X. Zhao and Q. Zhang, Polysulfide Electrocatalysis on Framework Porphyrin in High-Capacity and High-Stable Lithium–Sulfur Batteries, *CCS Chem.*, 2019, **1**, 128–137.

37 Z. Yuan, H. J. Peng, T. Z. Hou, J. Q. Huang, C. M. Chen, D. W. Wang, X. B. Cheng, F. Wei and Q. Zhang, Powering Lithium–Sulfur Battery Performance by Propelling Polysulfide Redox at Sulfiphilic Hosts, *Nano Lett.*, 2016, **16**, 519–527.

38 D. Ma, B. Hu, W. Wu, X. Liu, J. Zai, C. Shu, T. T. Tsega, L. Chen, X. Qian and T. L. Liu, Highly active nanostructured CoS_2/CoS heterojunction electrocatalysts for aqueous polysulfide/iodide redox flow batteries, *Nat. Commun.*, 2019, **10**, 3367.

39 S. D. Seo, D. Park, S. Park and D. W. Kim, "Brain-Coral-Like" Mesoporous Hollow CoS_2@N-Doped Graphitic Carbon Nanoshells as Efficient Sulfur Reservoirs for Lithium–Sulfur Batteries, *Adv. Funct. Mater.*, 2019, **29**, 1903712.

40 Q. Hu, J. Lu, C. Yang, C. Zhang, J. Hu, S. Chang, H. Dong, C. Wu, Y. Hong and L. Zhang, Promoting Reversible Redox Kinetics by Separator Architectures Based on CoS_2/HPGC Interlayer as Efficient Polysulfide-Trapping Shield for Li-S Batteries, *Small*, 2020, **16**, e2002046.

41 X. Zhao, M. Yang, J. Wang and D. Wang, Hollow Multishelled Structural Li-rich Cathode with Al Doping Enabling Capacity and Voltage Stabled Li-ion Batteries, *Chem. Res. Chin. Univ.*, 2023, **39**, 630–535.

42 R. Bi, D. Man, J. Wang, R. Yu and D. Wang, Hollow Nanostructures for Surface/Interface Chemical Energy Storage Application, *Acta Chim. Sin.*, 2020, **78**, 1200–1212.

43 D. Mao, C. Wang, W. Li, L. Zhou, J. Liu, Z. Zheng, Y. Zhao, A. Cao, S. Wang, J. Huang, F. Huo, H. Chen, L. Mai, R. Yu, L. Wang, Y. Lu, C. Yu, Q. Yang, Z. Yang, H. C. Zeng, H. Zhao, Z. Tang, D. Zhao and D. Wang, Hollow Multishelled Structure: Synthesis Chemistry and Application, *Chem. Res. Chin. Univ.*, 2024, **40**, 346–393.

44 J. Wang, Z. Wang, D. Mao and D. Wang, The development of hollow multishelled structure: from the innovation of synthetic method to the discovery of new characteristics, *Sci. China: Chem.*, 2021, **65**, 7–19.

45 F. Xie, L. Zhang, Q. Gu, D. Chao, M. Jaroniec and S. Z. Qiao, Multi-shell hollow structured Sb_2S_3 for sodium-ion batteries with enhanced energy density, *Nano Energy*, 2019, **60**, 591.

46 J. Wang, J. Wan and D. Wang, Hollow Multishelled Structures for Promising Applications: Understanding the Structure-Performance Correlation, *Acc. Chem. Res.*, 2019, **52**, 2169.

47 H. Wang, P. Wei, J. Wang and D. Wang, Hollow Multishelled Structure Reviving Lithium Metal Anode for High-energy-density Batteries, *Chem. Res. Chin. Univ.*, 2024, **40**, 428–436.

48 Z. Li, X. Lai, H. Wang, D. Mao, C. Xing and D. Wang, General Synthesis of Homogeneous Hollow Core−Shell Ferrite Microspheres, *J. Phys. Chem. C.*, 2009, **113**, 2792.

49 E. H. M. Salhabi, J. Zhao, J. Wang, M. Yang, B. Wang and D. Wang, Hollow Multi-Shelled Structural TiO_{2-x} with Multiple Spatial Confinement for Long-Life Lithium–Sulfur Batteries, *Angew. Chem., Int. Ed.*, 2019, **58**, 9078.

50 Y. Zhu, J. Wang, C. Xie, M. Yang, Z. Zheng and R. Yu, Hollow multishelled structural NiO as a "shelter" for high-performance Li-S batteries, *Mater. Chem. Front.*, 2020, **4**, 2971.

51 X. Han, X. Wu, Y. Deng, J. Liu, J. Lu, C. Zhong and W. Hu, Ultrafine Pt Nanoparticle-Decorated Pyrite-Type CoS_2 Nanosheet Arrays Coated on Carbon Cloth as a

Bifunctional Electrode for Overall Water Splitting, *Adv. Energy Mater.*, 2018, **8**, 1800935.

52 G. Ai, Q. Hu, L. Zhang, K. Dai, J. Wang, Z. Xu, Y. Huang, B. Zhang, D. Li, T. Zhang, G. Liu and W. Mao, Investigation of the Nanocrystal CoS_2 Embedded in 3D Honeycomb-like Graphitic Carbon with a Synergistic Effect for High-Performance Lithium Sulfur Batteries, *ACS Appl. Mater. Interfaces*, 2019, **11**, 33987.

53 J. Chen, H. Zhang, H. Yang, J. Lei, A. Naveed, J. Yang, Y. Nuli and J. Wang, Towards practical Li–S battery with dense and flexible electrode containing lean electrolyte, *Energy Storage Mater.*, 2020, **27**, 307–315.

54 Q. Zhao, R. Wang, J. Wen, X. Hu, Z. Li, M. Li, F. Pan and C. Xu, Separator engineering toward practical Li-S batteries: Targeted electrocatalytic sulfur conversion, lithium plating regulation, and thermal tolerance, *Nano Energy*, 2022, **95**, 106982.

55 M. Chen, M. Shao, J. Jin, L. Cui, H. Tu and X. Fu, Configurational and Structural Design of Separators toward Shuttling-Free and Dendrite-Free Lithium-Sulfur Batteries: A Review, *Energy Storage Mater.*, 2022, **47**, 629–648.

56 Z. Du, X. Chen, W. Hu, C. Chuang, S. Xie, A. Hu, W. Yan, X. Kong, X. Wu, H. Ji and L. J. Wan, Cobalt in Nitrogen-Doped Graphene as Single-Atom Catalyst for High-Sulfur Content Lithium-Sulfur Batteries, *J. Am. Chem. Soc.*, 2019, **141**, 3977.

57 D. Fang, Y. Wang, X. Liu, J. Yu, C. Qian, S. Chen, X. Wang and S. Zhang, Spider-Web-Inspired Nanocomposite-Modified Separator: Structural and Chemical Cooperativity Inhibiting the Shuttle Effect in Li-S Batteries, *ACS Nano*, 2019, **13**, 1563–1573.

58 W. Zhou, L. Ma, D. Zhao, J. Li, Z. Chen, W. Mai, N. Wang and L. Li, Crystal Surface Engineering Induced Active Hexagonal Co_2P-V_2O_3 for Highly Stable Lithium–Sulfur Batteries, *Small*, 2022, **18**, e2200405.

59 C. Cai, L. Wu, Z. Cai, F. Yu, L. Zhang, L. Wang, T. Mei, L. Lin and X. Wang, Self-assembly of Co-doped MnO_2 nanorod networks with abundant oxygen vacancy-modified separators for high-performance Li–S batteries, *Inorg. Chem. Front.*, 2023, **10**, 1775–1785.

60 J. Cai, Y. Song, X. Chen, Z. Sun, Y. Yi, J. Sun and Q. Zhang, MOF-Derived Conductive Carbon Nitrides for Separator-Modified Li–S Batteries and Flexible Supercapacitors, *J. Mater. Chem. A*, 2020, **8**, 1757–1766.

61 J. Xu, S. An, X. Song, Y. Cao, N. Wang, X. Qiu, Y. Zhang, J. Chen, X. Duan, J. Huang, W. Li and Y. Wang, Towards High Performance Li–S Batteries via Sulfonate-Rich COF-Modified Separator, *Adv. Mater.*, 2021, **33**, 2105178.

62 Z. Shen, Z. Zhang, M. Li, Y. Yuan, Y. Zhao, S. Zhang, C. Zhong, J. Zhu, J. Lu and H. Zhang, Rational Design of a $Ni_3N_{0.85}$ Electrocatalyst to Accelerate Polysulfide Conversion in Lithium–Sulfur Batteries, *ACS Nano*, 2020, **14**, 6673–6682.

63 R. Bi, N. Xu, H. Ren, N. Yang, Y. Sun, A. Cao, R. Yu and D. Wang, A Hollow Multi-Shelled Structure for Charge Transport and Active Sites in Lithium-Ion Capacitors, *Angew. Chem., Int. Ed.*, 2020, **59**, 4865.

64 J. Wang, N. Yang, H. Tang, Z. Dong, Q. Jin, M. Yang, D. Kisailus, H. Zhao, Z. Tang and D. Wang, Accurate control of multishelled Co_3O_4 hollow microspheres as high-performance anode materials in lithium-ion batteries, *Angew. Chem., Int. Ed.*, 2013, **52**, 6417.